A high-resolution record of early Paleozoic climate

Samuel L. Goldberg[a,1], Theodore M. Present[b], Seth Finnegan[c], and Kristin D. Bergmann[a]

[a]Department of Earth, Atmospheric, and Planetary Sciences, Massachusetts Institute of Technology, Cambridge, MA 02139; [b]Division of Geological and Planetary Sciences, California Institute of Technology, Pasadena, CA 91125; and [c]Department of Integrative Biology, University of California Berkeley, Berkeley, CA 94720

Edited by Mark Thiemens, University of California San Diego, La Jolla, CA, and approved January 11, 2021 (received for review July 6, 2020)

The spatial coverage and temporal resolution of the Early Paleozoic paleoclimate record are limited, primarily due to the paucity of well-preserved skeletal material commonly used for oxygen-isotope paleothermometry. Bulk-rock $\delta^{18}O$ datasets can provide broader coverage and higher resolution, but are prone to burial alteration. We assess the diagenetic character of two thick Cambro–Ordovician carbonate platforms with minimal to moderate burial by pairing clumped and bulk isotope analyses of micritic carbonates. Despite resetting of the clumped-isotope thermometer at both sites, our samples indicate relatively little change to their bulk $\delta^{18}O$ due to low fluid exchange. Consequently, both sequences preserve temporal trends in $\delta^{18}O$. Motivated by this result, we compile a global suite of bulk rock $\delta^{18}O$ data, stacking overlapping regional records to minimize diagenetic influences on overall trends. We find good agreement of bulk rock $\delta^{18}O$ with brachiopod and conodont $\delta^{18}O$ trends through time. Given evidence that the $\delta^{18}O$ value of seawater has not evolved substantially through the Phanerozoic, we interpret this record as primarily reflecting changes in tropical, nearshore seawater temperatures and only moderately modified by diagenesis. Focusing on the samples with the most enriched, and thus likely least-altered, $\delta^{18}O$ values, we reconstruct Late Cambrian warming, Early Ordovician extreme warmth, and cooling around the Early–Middle Ordovician boundary. Our record is consistent with models linking the Great Ordovician Biodiversification Event to cooling of previously very warm tropical oceans. In addition, our high-temporal-resolution record suggests previously unresolved transient warming and climate instability potentially associated with Late Ordovician tectonic events.

paleoclimate | Ordovician | oxygen isotope | biodiversification

The mid-Cambrian to Ordovician interval includes some of the most striking biodiversity changes in the history of life: the Great Ordovician Biodiversification Event (GOBE), following ∼40 million years (Myr) of relatively static biodiversity (1–4), and the Late Ordovician Mass Extinction, the first of the "Big Five" Phanerozoic extinctions (5). These events occurred in the context of a dynamic Earth system, and numerous causal linkages between Cambro-Ordovician Earth system changes and biodiversity trends have been proposed. It has been argued that the GOBE occurred in response to climatic cooling and consequent relaxation of physiological stressors (6, 7) and that the end-Ordovician extinction was linked to Gondwanan glaciation, either through the combined effects of cooling and sea-level fall (8) or through associated changes in ocean ventilation (9, 10). These climatic changes are argued to have been linked to increased orogenesis, arc accretion, and ophiolite obduction through the effects of volcanism and/or silicate weathering on atmospheric pCO_2 (11–13). The evolution and expansion of early land plants may also have played a role by changing the dynamics of silicate weathering and organic carbon sequestration (14).

Testing hypotheses regarding the interactions among tectonics, climate, and evolution requires reliable records of each. Fossils provide a rich record of marine biodiversity through early Phanerozoic time (1), and tectonic history has been reconstructed, at least in part, from multiple lines of geological evidence (12), but early Paleozoic climate history is less well constrained (15, 16). The most commonly used proxy for ancient climate is the mineral oxygen-isotope thermometer, which relies on the temperature-dependent equilibrium fractionation between minerals and water (17). This proxy has been widely applied in the geologic record, but has two major limitations when applied to the early Paleozoic. First, the oxygen-isotopic composition of minerals is a function both of the temperature-dependent fractionation and of the composition of the precipitating fluid, so determination of precipitation temperature requires either external constraints or assumptions of ancient seawater composition. Second, past Paleozoic paleoclimate reconstructions have utilized $\delta^{18}O$ values of carbonate or phosphate shells of marine animals (brachiopods and conodonts) because they were precipitated from seawater and can be carefully screened for diagenetic alteration (6, 8, 18–22), but well-preserved fossils are sparse in Cambrian and Early Ordovician sedimentary rocks (23).

Progress has been made on the first limitation for early Phanerozoic paleoclimate reconstruction. While $\delta^{18}O$ values of early Paleozoic carbonates are consistently lower than modern carbonates, interpretation of this difference has been the focus of longstanding controversy. Three end-member hypotheses have been proposed, with diverging implications for climate history (20, 22, 24, 25). One hypothesis is that this difference reflects precipitation from oceans that were isotopically similar to, but warmer than, modern oceans. Alternatively, lower $\delta^{18}O$ values could reflect precipitation at modern-like temperatures from ancient oceans that had lower $\delta^{18}O$ compositions than modern. Finally, these values could reflect diagenetic oxygen exchange under burial conditions and, thus, not be indicative of surface conditions (temperature or seawater composition). The relative influence of these three effects cannot be

Significance

The Cambrian–Ordovician (541 million to 443 million y ago) climate record is poorly constrained due to the sparsity of carbonate fossils typically used for temperature reconstructions. We demonstrate that the abundant carbonate sediments from this time can preserve isotopic compositions and trends similar to those of fossil material and combine sediment records into a high-resolution proxy record of Late Cambrian and Ordovician climate. Examination of this record in the context of evolutionary and tectonic changes demonstrates that Earth's climate was tightly coupled to tectonic and volcanic activity and played a strong role in biodiversity trends during the time of early animal evolution.

Author contributions: S.L.G. and K.D.B. designed research; S.L.G., S.F., and K.D.B. performed research; S.L.G., T.M.P., S.F., and K.D.B. analyzed data; and S.L.G., T.M.P., S.F., and K.D.B. wrote the paper.

The authors declare no competing interest.

This article is a PNAS Direct Submission.

Published under the PNAS license.

[1]To whom correspondence may be addressed. Email: sgoldberg@mit.edu.

This article contains supporting information online at https://www.pnas.org/lookup/suppl/doi:10.1073/pnas.2013083118/-/DCSupplemental.

Published February 1, 2021.

Downloaded at CALIFORNIA INST OF TECHNOLOGY on February 1, 2021

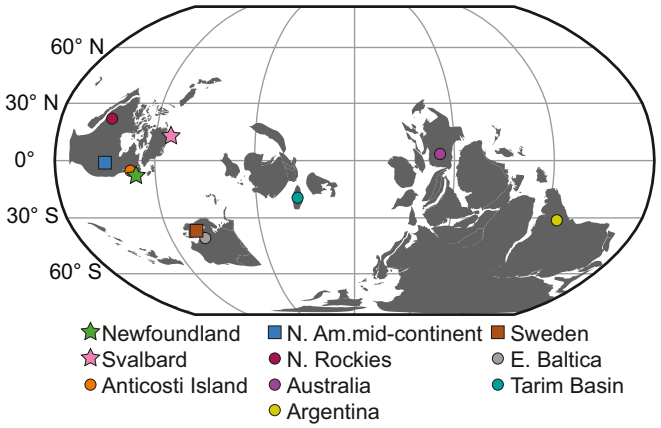

Fig. 1. Paleogeographic locations (465 Ma) of locations analyzed in this study. Stars denote locations of our micrite measurements, squares our brachiopod measurements, and circles compiled literature data. Plate reconstruction is from ref. 11. Am., American; E., East; N., North.

disentangled with the oxygen-isotope system alone. Clumped-isotope studies of well-preserved fossil skeletal materials, which can constrain mineral-formation temperatures independently of the isotopic composition of the precipitating fluid (26, 27), have consistently reconstructed Paleozoic seawater oxygen-isotopic compositions as similar to Cenozoic ice-free oceans (8, 20), except for ice-volume effects or local evaporative enrichment. This result is consistent with carbonate clumped-isotope analyses of Ediacaran bulk carbonate rocks (28), oxygen-isotope analyses of iron oxide precipitates (29), and hydrothermal alteration minerals in ophiolites (30, 31). Based on these findings, we interpret the depletion of oxygen-isotope records from the early Paleozoic to reflect a combination of climatic variability, diagenesis, evaporative enrichment, and ice-volume changes, and not a long-term, secular change in the bulk oxygen-isotopic composition of seawater from very negative ancient values (e.g., ref. 25).

Here, we focus on addressing the second limitation in reconstructing early Paleozoic climate: the paucity of fossil materials from which to generate a high-resolution oxygen-isotope record. Carbonate sediments are abundant throughout this interval and can be used to produce oxygen-isotope records of both higher spatial and temporal resolution than the early Paleozoic skeletal fossil record. Carbonate sediments are less explored as a paleothermometer than skeletal carbonates because of their uncertain provenance, assumed high potential for postdepositional alteration, and the relative difficulty of assessing their alteration history. We test the validity of this assumption and explore the use of early Paleozoic bulk carbonate oxygen isotopes as recorders of past surface conditions.

We present paired clumped and bulk isotopic measurements of micritic samples from two long-lived and well-preserved portions of an early Paleozoic carbonate platform on the Laurentian margin, in Svalbard and Newfoundland, and find evidence that, due to low fluid availability during burial, their oxygen-isotopic compositions have largely been retained despite diagenetic resetting of the clumped-isotope thermometer. Motivated by this result, we then compile oxygen-isotope bulk rock measurements from seven globally distributed, largely tropical, Cambrian–Ordovician carbonate platforms (Fig. 1), align these records biostratigraphically (*Materials and Methods*), and assess their agreement and consistency. To minimize local effects and diagenesis, we average regional records into a global oxygen-isotope stack, similar to efforts for the more recent geologic past (32). As an external test of its accuracy, we compare our stacked bulk rock oxygen-isotope record with lower-resolution brachiopod and conodont oxygen-isotope records, thought to be more robust to diagenetic alteration and long used as Paleozoic climate proxies (6, 22).

Clumped-Isotope Systematics

Clumped-isotope Δ_{47} analyses of our micrite samples from both Svalbard (Fig. 2, *SI Appendix*, Fig. S1, and Dataset S1) and Newfoundland (Fig. 2, *SI Appendix*, Fig. S2, and Dataset S2) imply diagenetic alteration under relatively shallow burial conditions (33). Clumped-isotope temperatures (45 to 100 °C) are elevated above the range of plausible surface temperatures (Fig. 2). These measured temperatures could reflect a range of processes, including early precipitated micrite that lithified with secondary cements precipitated at elevated temperatures, dissolution and reprecipitation of primary carbonate material, and/or partial solid-state bond reordering during exposure to temperatures below the calcite-blocking temperature (34). These clumped-isotope temperatures are less than or comparable to peak burial temperatures suggested by previous studies of other thermally sensitive proxies. Studies of Ny Friesland, Svalbard, report the preservation of biomarkers at midoil window maturity with organic Tmax values of 441 to 446 °C (35) and conodont alteration indices (CAIs) of 1 to 1.5 (36), both indicating burial of <4 km and peak burial temperatures <150 °C (37). Similar studies of the Port au Port Peninsula, Newfoundland, report fluid inclusion temperatures of 67 to 77 °C, thermally immature biomarkers (38), and CAI of one (39), suggesting burial of <3 km and peak burial temperatures <100 °C. In both sections, partial alteration of clumped-isotope temperatures during burial is implied by the overlapping distributions of temperatures from micrites and cross-cutting calcite veins, despite clear differences in bulk oxygen isotopes of each component (Fig. 2). We use fractionation relationships and our measured clumped-isotope temperatures to estimate the $\delta^{18}O$ values of water in equilibrium

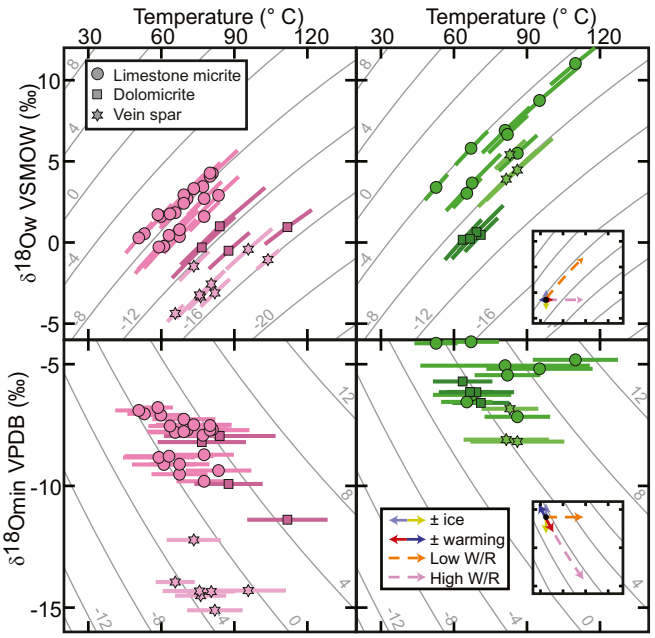

Fig. 2. Comparison of clumped-isotope temperature, mineral $\delta^{18}O$, and fluid $\delta^{18}O$ for analyzed samples from Svalbard (*Left*) and Newfoundland (*Right*). Symbols denote mineralogy, and colors denote sample location as in Fig. 1. (*Insets*) Theoretical trajectories for variations in surface conditions (solid lines) and diagenetic pathways (dashed lines). Gray lines in each plot are constant contours of the third, unplotted variable for calcite equilibrium fractionation. W/R, water/rock ratio. Adapted with permission from ref. 28.

Downloaded at CALIFORNIA INST OF TECHNOLOGY on February 1, 2021

with the observed micrite $\delta^{18}O$ values (*Materials and Methods*), giving fluid $\delta^{18}O$ values ranging from 0‰ Vienna Standard Mean Ocean Water (VSMOW) (consistent with modern seawater) to 11‰ VSMOW (consistent with burial fluids buffered by carbonate minerals) (Fig. 2). Partial solid-state bond reordering, if it occurred, would bias estimated fluid $\delta^{18}O$ toward higher values, since this process does not involve exchange between bulk carbonate and water. In Svalbard, the low fluid $\delta^{18}O$ composition (<0‰ VSMOW) from which the vein calcite precipitated likely represents secondary, meteoric fluids.

The Newfoundland section records both higher $\delta^{18}O$ values and cooler Δ_{47} temperatures in the Cambrian Port au Port group than in Early Ordovician strata, while Late Ordovician samples record even higher $\delta^{18}O$ values and cooler Δ_{47} temperatures than Cambrian samples, a pattern inconsistent with complete resetting of clumped-isotope temperature during burial and, thus, indicating at least partial preservation of clumped-isotope and bulk isotopic compositions. Similarly, Neoproterozoic strata in Ny Friesland record comparable or colder clumped-isotope temperatures to the Oslobreen Group, despite their greater overburden (37). The partial preservation of stratigraphic Δ_{47} trends that align with $\delta^{18}O$ trends likely indicates some preservation of primary or very early diagenetic mineral material that is either diluted by secondary cements or affected by partial solid-state reordering. The scatter among nearby samples in the Svalbard section may reflect the variable contribution of primary and secondary material.

Clumped-Isotope Constraints on Diagenesis and Preservation of the Oxygen-Isotope Record

Because different oxygen-isotope alteration mechanisms have predictable consequences for the stable isotope evolution of carbonate minerals (28), clumped-isotope data provide critical constraints on whether bulk $\delta^{18}O$ values have been substantially altered by exchange with fluids in an open system (high water/rock ratio) or preserved in a closed system (low water/rock ratio) (Fig. 2, *Inset*). Results from Newfoundland and Svalbard follow broadly similar geochemical trajectories in clumped-isotope temperature, mineral $\delta^{18}O$ value, and equilibrium fluid $\delta^{18}O$ value space (Fig. 2), indicating that they experienced diagenetic alteration in a relatively closed system. Open-system fluid-buffered dissolution and reprecipitation at 80 °C (from clumped-isotope temperatures) by marine fluids with a $\delta^{18}O$ composition of −1.4‰ [typical Paleozoic ice-free value (20)] would yield a mineral $\delta^{18}O$ value of −13.1‰ Vienna Pee Dee Belemnite (VPDB); this is the expectation for complete, open-system diagenetic overprinting of primary mineral $\delta^{18}O$ values at the clumped-isotope temperatures recorded by our samples. However, mean $\delta^{18}O$ compositions of micritic samples are −5.6‰ and −8.2‰ VPDB for Newfoundland and Svalbard, respectively, implying that alteration of these strata occurred primarily in a more closed system with minimal fluid exchange under rock-buffered conditions (i.e., with a low water/rock ratio). Under such conditions, fluid compositions evolve toward rock values as diagenesis proceeds, thus explaining the enriched fluid compositions (0 to 11‰ VSMOW) inferred for our samples and the correlation between temperature and fluid composition along contours of constant mineral $\delta^{18}O$ values (Fig. 2).

Micrite samples from Svalbard are generally 2 to 3‰ more depleted in $\delta^{18}O$ compared to the Newfoundland samples, indicating that they likely experienced relatively higher water/rock ratios and greater fluid interaction during diagenesis. This inference is supported by the observation that calcite veins are ubiquitous throughout the Svalbard section, but largely absent from the Newfoundland strata, except in the vicinity of faults. Although the Svalbard sample array implies greater water/rock ratios than the Newfoundland array, both sample suites have much higher bulk $\delta^{18}O$ compositions than would be expected under fully fluid-buffered equilibration at burial conditions. $\delta^{18}O$ values of micritic samples from Svalbard are similar to those of ocular calcite in fossil trilobites from this section (40) and substantially different from those of adjacent vein-hosted calcite spar.

Closed-system diagenetic alteration under low water/rock ratios limits the magnitude of possible change to bulk mineral $\delta^{18}O$ during fluid–rock interaction, with changes to fluid composition far exceeding changes in bulk carbonate composition during burial equilibration. Even with some alteration, stratigraphic trends in $\delta^{18}O$ will be largely preserved if all rocks in a given section experienced similar diagenetic processes and fluid availability. This assumption may be violated by stratigraphic changes in physical properties such as porosity or permeability that influence fluid flow, but we minimize this concern by consistently targeting micritic mudstone microfacies. Our analyses consequently suggest that $\delta^{18}O$ trends in these two sections are dominated by primary signals, with moderate secondary diagenetic noise (6, 19, 22, 41, 42). High-resolution $\delta^{18}O$ records have been previously collected for these strata, and our samples span most of the previously reported $\delta^{18}O$ range (*SI Appendix*, Fig. S4), indicating that the closed-system diagenetic systematics indicated by our samples are broadly representative of the regional geology. We therefore posit that the similar temporal trends of increasingly enriched $\delta^{18}O$ values toward the end-Ordovician in Newfoundland and Svalbard reflect a common underlying primary signal, although higher-resolution $\delta^{18}O$ records may capture variability not seen in our data (such as high $\delta^{18}O$ values in Dapingian strata in Newfoundland).

Compiling a High-Resolution Cambrian–Ordovician Global $\delta^{18}O$ Record

Clumped-isotope measurements from Anticosti Island, Québec, the Laurentian midcontinent (upper Mississippi Valley and Cincinnati Arch), and Baltica (Estonia and Russia) (8, 20) indicate that these basins also experienced rock-buffered diagenetic alteration, and it occurred at lower burial temperatures than our Newfoundland and Svalbard sections. We report brachiopod clumped-isotope data from the Late Ordovician (Katian) of the Laurentian midcontinent and the early Silurian of Gotland (*SI Appendix*, Fig. S3 and Dataset S3) that corroborate previous findings (20, 43) and give further evidence that these basins experienced low water/rock diagenesis. Paired $\delta^{18}O$ and clumped-isotope analyses indicate that, while imperfect due to locally variable diagenetic overprint, the bulk oxygen-isotopic composition of ancient carbonate sediments deposited in thick carbonate platforms may still be dominated by a primary signal and should be explored.

We stack $\delta^{18}O$ records from these and other well-preserved basins to reduce the influence of local environmental and diagenetic effects and produce a single, global, shallow tropical $\delta^{18}O$ record. In addition to our data from Svalbard and Newfoundland, we selected limestone-dominated carbonate records that we assess as likely to have been well-preserved based on other constraints. We include Anticosti Island, Laurentian midcontinent, and Baltica, which have previously yielded low clumped-isotope temperatures (8, 20); and the Argentine Precordillera (44–47), central Sweden (48, 49), and the Tarim Basin (China) (50), which have well-preserved brachiopod fossils (22) (Fig. 3 and *SI Appendix*, Fig. S4) (see *Materials and Methods* for all data sources). We exclude data from dolostone-dominated or shale-dominated lithologies and additionally excluded one dataset with anomalously low $\delta^{18}O$ values that imply alteration under high water/rock ratios (*Materials and Methods*).

Consistent $\delta^{18}O$ trends across different regions in both bulk carbonates and fossils suggest that these records are dominated

Downloaded at CALIFORNIA INST OF TECHNOLOGY on February 1, 2021

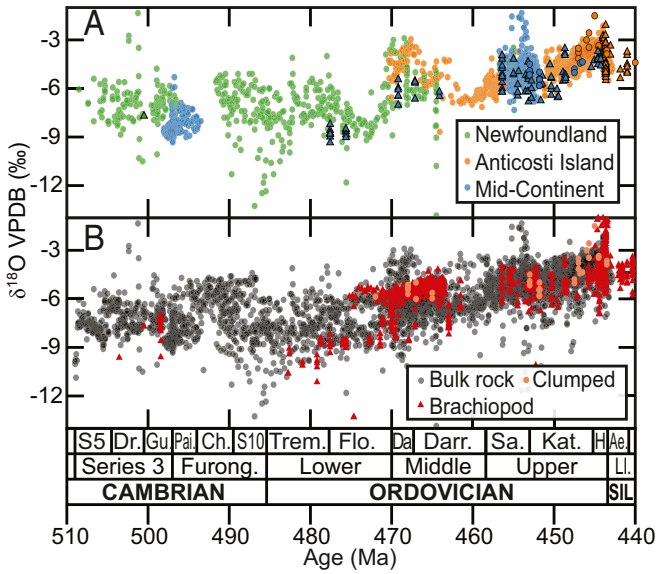

Fig. 3. Comparison of bulk rock and fossil oxygen-isotope data. (*A*) Data from North American samples, colored by location as in Fig. 1. Circles denote bulk rock, triangles denote brachiopod samples (22), and outlined circles denote δ^{18}O from clumped-isotope samples (20). (*B*) Global data. Black circles are bulk rock, red triangles are brachiopod (22), and orange circles denote δ^{18}O from clumped-isotope samples (20).

by a shared primary signal. To test the correlation of our records, we combine datasets from Newfoundland and Anticosti Island into a single long-duration record from the Laurentian eastern margin and find that the majority of other regional records, when compared by time-binned average (*Materials and Methods*) to this Laurentian record, exhibit a positive and statistically significant ($P < 0.05$) correlation (*SI Appendix*, Fig. S5). Of all 19 pairwise correlations, we find a majority of positive correlations and that positive and significant correlations (8) are much more common than negative and significant correlations (2). As an external test, we compare our rock δ^{18}O records to measurements of brachiopod calcite and conodont apatite (6, 22, 41, 42). Laurentian bulk δ^{18}O data are consistent with the available brachiopod data and with one another (Fig. 3*A*). Other locations for which both fossil data and bulk rock records are available (Baltica and Tarim Basin) also show general temporal consistency between the two proxy records (*SI Appendix*, Fig. S4), as does the full global compilation (Fig. 3*B* and *SI Appendix*, Fig. S6). Given the tendency of diagenetic alteration toward lower values, we interpret the highest δ^{18}O values for a location as closest to primary mineral compositions.

To calculate temperatures from this global bulk rock δ^{18}O record, we use a model for seawater composition based on minimum clumped-isotope constraints from well-preserved fossils (8, 20), featuring a fluid δ^{18}O value that is -1.4‰ VSMOW for much of the Ordovician and increases during Late Ordovician glaciation because of ice-volume-driven changes (*SI Appendix*, Fig. S7). We combine this inferred seawater δ^{18}O history with the bulk rock δ^{18}O stack to extract a surface temperature record (Fig. 4*B*) (*Materials and Methods*). To visualize the spread of calculated temperatures, we compute deciles (10th to 90th percentiles) for the global compilation (Fig. 4*B*) (*Materials and Methods*). Because alteration typically shifts δ^{18}O values lower (toward higher inferred temperatures), we interpret the lowest deciles of our temperature record as the closest approximation to coastal, tropical temperatures; implausibly warm temperatures in the highest deciles likely reflect diagenetic alteration. Our global temperature compilation from calcite rocks is consistent with the long-term Ordovician cooling trend inferred from both brachiopod calcite and conodont apatite δ^{18}O (Fig. 4*B*) (6).

Compared to the deep-sea benthic records and open-ocean planktonic records used to reconstruct Cenozoic climate history (57, 58), shallow-water coastal settings like those dominating

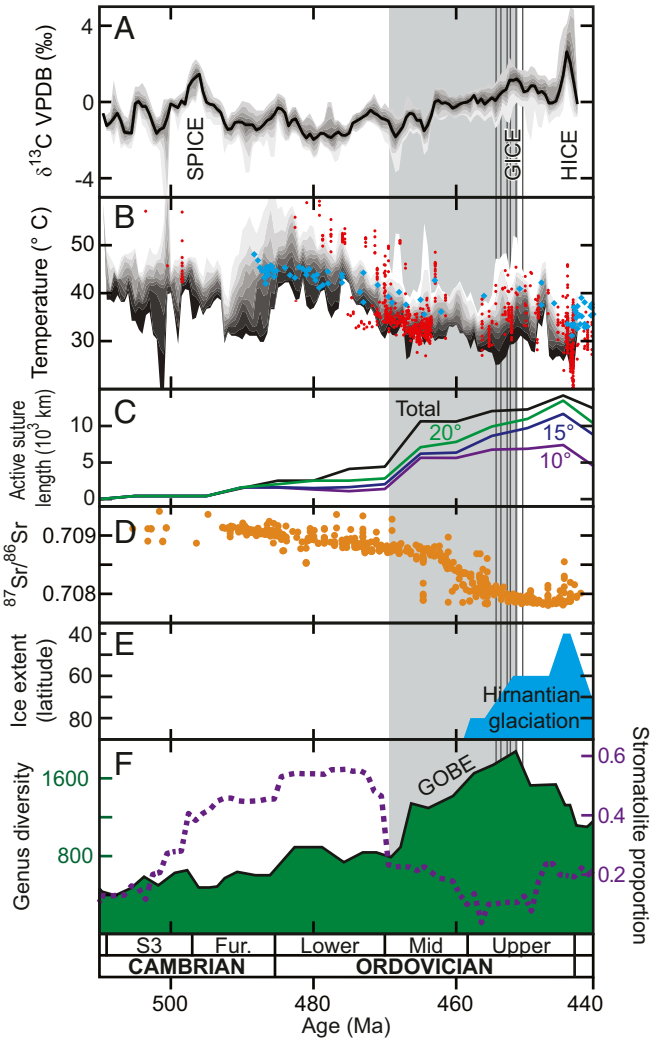

Fig. 4. Climatic and tectonic context of early animal evolution, with evolutionary events highlighted. (*A*) Bulk rock δ^{13}C from our literature data compilation, with key excursions highlighted. GICE, Guttenberg δ^{13}C Excursion; HICE, Hirnantian δ^{13}C Excursion; SPICE, Steptoean Positive Carbon Isotope excursion. (*B*) Oxygen-isotope-derived temperature; the shading denotes the deciles of all global data to indicate the spread of the data. The darker regions correspond to the more ^{18}O-enriched (lower temperature) portion of the distribution, which is expected to represent less diagenetic alteration. Small red points are temperature from brachiopod δ^{18}O , and blue diamonds are temperature from conodont apatite δ^{18}O (*Materials and Methods*). (*C*) Length of active tectonic sutures (12). Total active length is shown with the black line and points; colored points and lines denote active length within the tropics (10°, 15°, and 20° from the equator). (*D*) Strontium isotope ratio, a proxy for continental weathering (51, 52). (*E*) Latitudinal extent of glaciation (12). (*F*) The green curve shows marine genus diversity (left axis), from the model of ref. 1. The dashed purple line shows the proportion of marine carbonate units containing stromatolites (right axis) (53). The vertical gray bar shows the GOBE interval; thin vertical lines denote the ages of widespread K-bentonites (54–56).

Downloaded at CALIFORNIA INST OF TECHNOLOGY on February 1, 2021

the Cambrian–Ordovician stratigraphic record are typically warmer and exhibit more regional and seasonal temperature variation (59). These records may also be influenced by local conditions, since surface temperatures vary as a function of latitude and basin geometry, and seawater $\delta^{18}O$ values in modern surface waters can vary by up to ~5‰ (60). Our use of a global $\delta^{18}O$ value for seawater is thus a simplifying assumption, and some of the $\delta^{18}O$ variability among regions may derive from primary surface ocean temperature and water-composition heterogeneity, in addition to secondary diagenetic modification.

Interpreting the lowest deciles of the bulk $\delta^{18}O$ compilation as a paleotemperature proxy, we reconstruct Early Ordovician (Tremadocian–Floian) temperatures warmer than either the preceding late Cambrian time or the subsequent Middle and Late Ordovician epochs. This warm interval is followed by cooling of ~10 to 15 °C through the Floian–Dapingian at a rate of ~1° C/Myr. This record of cooling over a relatively narrow interval contrasts with protracted cooling over the entire Early and Middle Ordovician epochs reconstructed by ref. 6, but the global composite temperature drop we reconstruct is more protracted than that reconstructed for Baltica by ref. 7. The magnitude of Early–Middle Ordovician cooling (10 to 15 °C) is similar to the cooling of deep waters during the Cenozoic hothouse–icehouse transition (61), though it is difficult to compare the records directly because our record reflects temperatures in shallow coastal environments. While Late Ordovician temperature estimates after 467 million years before present (Ma) are sensitive to modeled ice-sheet growth (*SI Appendix*, Figs. S7 and S8), our compiled data suggest warming from ~454 to 449 Ma, followed by a return to cooler temperatures preceding onset of the Hirnantian icehouse state (Fig. 4).

Implications for Other Earth Systems

Our stacked record can be compared to similarly high-resolution records of biodiversity (1) and tectonic activity (12) to evaluate hypotheses regarding interactions between tectonics, climate, and biodiversity (Fig. 4). High temperatures across the Cambrian/Ordovician boundary and in the Early Ordovician epoch may have been an important driver of the high rates of species turnover (1), potentially exacerbated by the negative relationship between water temperature and dissolved oxygen and consequent widespread anoxia in Late Cambrian and Early Ordovician shallow oceans (3, 62). As argued by ref. 6, subsequent cooling across the Early/Middle Ordovician boundary may have helped to trigger the GOBE through the combined effects of cooler temperatures and increased ocean oxygenation (62). Like ref. 7, our record suggests cooling over a narrow time interval aligned with the main pulse of the GOBE in Baltica and Laurentia. We also see an increase in $\delta^{13}C$ values associated with cooling (Fig. 4*A*), both with the long-term Middle and Late Ordovician trend and the large excursion broadly associated with the Hirnantian icehouse. The abundance of stromatolites (53) exhibits a trend similar to the temperature record and is inversely correlated with animal biodiversity (Fig. 4*F*), increasing during Late Cambrian warming and decreasing at the Early–Middle Ordovician boundary, coincident with cooling and the onset of the GOBE. The correlation of temperature with biodiversity records suggests the influence of climate and related factors (e.g., seawater oxygenation) on the relative abundance and diversity of microbial and metazoan life.

Tectonic activity may be the ultimate driver of early Paleozoic climate and, hence, biodiversity trends. Cooling Middle Ordovician temperatures coincide with an increase in arc accretion (Fig. 4*C*), in agreement with proposed tectonic models for cooling (12), but precede the shift in strontium isotopes toward less radiogenic values (Fig. 4*D*); this lag may represent the long marine residence time of Sr (11). The brief warm interval that punctuates the Late Ordovician epoch is associated with repeated regional volcanic events, evidenced by the widespread deposition of well-dated K-bentonite ash layers (54–55, 63) and mercury chemostratigraphy (64–66). These volcanic eruptions may have led to enhanced climatic volatility, as perhaps evidenced by the regional "Boda event," which has been linked to warming (67). Volcanism can cause both warming from direct CO_2 emissions and cooling from silicate weathering and resulting CO_2 drawdown (11, 12, 68). The apparent increase in climate variability coincides with the end of the GOBE, beginning a protracted 8-Myr decline in biodiversity that culminates in the Hirnantian glacial maximum and mass extinction.

Conclusions

Clumped-isotope analyses of samples from Newfoundland and Svalbard demonstrate that the diagenetic alteration of these samples has had a minor impact on their oxygen-isotope composition. This finding, combined with prior work demonstrating the long-term stability of seawater oxygen-isotope composition, suggests that early Paleozoic $\delta^{18}O$ records are often dominated by a primary paleotemperature signal. We estimate global climate trends by stacking globally distributed datasets to minimize the effects of diagenesis and varying local conditions. Although we do not have clumped-isotope data for all locations, this interpretation is supported by the consistency of temporal trends among locations and the agreement between bulk rock data and fossil material regionally and in global compilations. Our global composite temperature curve shows Late Cambrian warming, Early Ordovician elevated temperatures, cooling leading into the Middle Ordovician epoch, and possibly enhanced climate volatility in the Late Ordovician epoch preceding the Hirnantian glaciation. Comparison with biodiversity reconstructions supports models linking global marine biodiversity to climate, with elevated temperatures and climate instability limiting metazoan diversity and cooler temperatures promoting metazoan diversification. The framework we lay out here can be used to vet, compile, and interpret $\delta^{18}O$ records for other time intervals that lack reliable biomineralized records, although this may be hindered by increasing cumulative diagenesis in deeper Earth history. In particular, the Precambrian climate record remains poorly constrained, but is critical to understanding the feedbacks among tectonics, climate, and the evolution of early life.

Supporting Information

Figs. S1–S8 are provided in *SI Appendix*.

SI Datasets. Clumped-isotope replicate measurements are provided in Dataset S1 (Svalbard), Dataset S2 (Newfoundland), and Dataset S3 (new brachiopod data).

Materials and Methods

Geologic Setting of Carbonate Samples. The micritic carbonate samples analyzed in this study were sourced from two locations: Ny Friesland (Svalbard) and Port au Port Peninsula (Newfoundland, Canada). The Svalbard samples (*SI Appendix*, Fig. S1) were collected in summer 2016 from northeast Ny Friesland, from the Cambrian and Ordovician Oslobreen Group (69, 70). This succession was deposited on the Laurentian passive margin bordering the Iapetus Ocean and overlies the Ediacaran Dracoisen Formation (70, 71). The ~1,000 m of stratigraphy are divided into the Tokammane, Kyrtonryggen, and Valhallfonna formations. Lithologically, these strata consist largely of limestone with minor dolostone, generally fossil-bearing, with horizons of ooids and stromatolites. The lower Olenidsletta Member of the Valhallfonna Formation is dark, thinly bedded, and rich in organic matter. The present-day Svalbard archipelago experienced regional tectonic deformation during the closure of the Iapetus Ocean as part of the Caledonian orogeny (72). The rifting of the Atlantic Ocean brought Svalbard to its present location

Downloaded at CALIFORNIA INST OF TECHNOLOGY on February 1, 2021

Table 1. Data sources for literature compilation

Location	Reference(s)
Newfoundland	(91–93)
Anticosti Island	(94, 95)
Sweden	(48, 49)
Svalbard	(36)
North America midcontinent	(43, 96, 97)
East Baltica (Estonia and Russia)	(7, 98, 99)
Tarim Basin	(50)
Argentine Precordillera	(44–47)

on the northern margin of the Eurasian Plate. Despite regional deformation, northeast Ny Friesland provides a window of relatively well-preserved strata. This locality is at the western edge of the Nordaustlandet terrane, which increases in burial grade eastward. Shallow burial is evidenced by low CAIs (36), as well as by abundant organic biomarkers that indicate midoil window thermal maturity (35).

Newfoundland samples (*SI Appendix*, Fig. S2) were collected in September 2017 from quarry outcrops and coastal exposures of the Port au Port, St. George, Table Head, and Long Point groups from the Port au Port Peninsula in western Newfoundland. The Middle–Upper Cambrian Port au Port and Lower Ordovician St. George groups were deposited on a long-lived, low-latitude carbonate platform on the Iapetan passive margin of Laurentia (73, 74). The platformal succession forms ∼1,000 m of stratigraphy on the Port au Port Peninsula. The Middle Ordovician Table Head, Goose Tickle, and Upper Ordovician Long Point groups are laterally heterogeneous foreland basin sediments recording the collapse of the carbonate platform and the deepening of the basin in response to the approaching Taconic arc (75, 76). The Laurentian margin experienced subsequent tectonic deformation during the Taconic, Salinic, and Acadian orogenies (77, 78), although evidence suggests that the Port au Port Peninsula experienced relatively little tectonic burial. Organic thermal maturity indicates burial by 1 to 1.5 km, with relatively thin overlying allochthonous thrust sheets (38). Thermal maturity increases eastward and northward with increasing tectonic burial and deformation. This is consistent with CAIs of one on the Port au Port Peninsula and two to three elsewhere (39); the Port au Port Peninsula preserves a window of shallow burial on a deformed margin.

Upper Ordovician brachiopod samples were collected from the Lexington and Waynesville formations at the South Gate Hill roadcut on Indiana Route 1 near Cedar Grove, Indiana, by K.D.B., S.F., and others (20). These mixed carbonate-siliciclastic formations deposited in a shallow epicontinental sea in the foreland basin of the Taconic Orogeny as a high-energy subtidal skeletal wackestone-packstone and as low-energy peritidal mudstone and shale, respectively (79, 80). Lower Silurian samples were collected from the Lower Visby Formation and Slite Group in Gotland, Sweden, by S.F. (20). These carbonate ramp units formed on slowly subsiding craton between two foreland basins during the Scandian Orogeny (81, 82).

Carbonate Stable Isotope Analysis. Rock samples were cut and polished to expose fresh, unweathered surfaces. Powders for analysis were extracted by drilling within uniform microfacies, micrite unless otherwise specified as spar, using a rotary drill press and a carbide drill bit. Sample mineralogy was assessed qualitatively by dilute acid reaction.

Brachiopod sampling targeted the best-preserved secondary fibrous layer calcite. Flakes of brachiopod calcite were separated from recrystallized calcite, cements, pyrite, iron oxides, and matrix material with a dental pick and tweezers under a binocular microscope (19, 83). Two to 80 mg of material was obtained from each brachiopod. Brachiopods were variably well-preserved and were assigned a visual preservation score from zero (best) to four (worst) that was the number of diagenetic features observed at ×50 magnification, including recrystallized (nonfibrous) calcite, residual matrix or cement, discoloration, and mineral (likely pyrite or iron oxide) inclusions; no sample had more than two observed diagenetic features. From each set of flakes, duplicate or triplicate aliquots of 3 to 5 mg were crushed into powder for geochemical analysis with an agate mortar and pestle.

Samples were analyzed for bulk and clumped isotopic composition in the Massachusetts Institute of Technology clumped-isotope laboratory with a NuCarb automated sample preparation system and a Nu Perspective dual-inlet gas-source isotope ratio mass spectrometer. Sample powders (60 to 100 μg for bulk isotope analysis only, 400 to 500 μg for clumped) were reacted for 20 min with 150 μL of orthophosphoric acid (density 1.93 g/cm^3) in single evacuated vials at 70 °C; the evolved CO_2 gas was purified cryogenically and by passage through a Porapak® filter at −30 °C. The purified sample gas was measured at *m/z* 44 to 49 in 60 cycles of 30 s each, in alternation with equal measurement of a reference gas of known composition, for a total integration time of 30 min per sample replicate. Unknown samples were run in parallel with carbonate standards of known bulk and clumped isotopic composition.

The raw mass-spectrometer data were reduced with Easotope software (84) and corrected to four ETH carbonate standards, following the method of refs. 37 and 85. Bulk isotope SD for carbonate standards was <0.1‰ for $\delta^{13}C$ and <0.2‰ for $\delta^{18}O$. Internal precision for Δ_{47} for the carbonate standards ranged from 0.01 to 0.04‰. The clumped-isotope equilibration temperature was calculated from Δ_{47} with the calibration of (85); the precipitating fluid composition was calculated with the fractionation relations of (86) (calcite) and (87) (dolomite). The bulk oxygen-isotope temperature was calculated with the same fractionation relations, using a time-dependent seawater isotopic composition from clumped-isotope studies (*SI Appendix*, Fig. S7) (8, 20).

Literature Data Compilation. Carbonate bulk isotope data were gathered from published papers (Table 1). Locations were selected with long records and without significant diagenetic alteration. We omitted a record from Sweden (88) that showed unusually depleted values, as well as a dolomitic record from India that was influenced by Himalayan orogeny (89). Data for each location were condensed with a 1-Myr centered moving median (*SI Appendix*, Figs. S4 and S6), computed every 500,000 y. A global average was computed as the mean of each location's moving median to avoid undue weighting by sample resolution. For comparison, we also compiled temperature data from oxygen-isotope analysis of conodont apatite (6, 41, 42), brachiopod calcite (22), and carbonate clumped-isotope thermometry (20). Carbonate temperatures were computed by using the calcite fractionation of ref. 86. Conodont apatite temperatures were recalculated by using the calibration of ref. 90.

Age Model. Samples were assigned chronometric ages by using reported biostratigraphic constraints, using the chronometric ages of the 2012 Geologic Time Scale (100, 101). Global stage boundaries were the primary age control points used when available; regional stages and biozones were used where global stages were not reported/available. Ages were interpolated assuming constant sedimentation rates between age control points. For references where ages were reported with chemical data, the authors' original ages were used.

Seawater Oxygen-Isotope Curve. Our seawater oxygen-isotope history (*SI Appendix*, Fig. S7), used to compute temperature from mineral $\delta^{18}O$, was constructed from clumped-isotope analyses of well-preserved fossil material reported by refs. 8 and 20. We conservatively used the most depleted reported water $\delta^{18}O$ as our constraints, as a minimum bound on seawater enrichment from ice-volume effects. We used a value of −1.4‰ VSMOW for the ice-free interval prior to 458 Ma (20).

Data Availability. Clumped-isotope measurements are available in Datasets S1–S3 and in the EarthChem repository (DOI: 10.26022/IEDA/111716).

ACKNOWLEDGMENTS. Fieldwork in Newfoundland was conducted by Samuel Goldberg, Marjorie Cantine, and Kristin Bergmann. Fieldwork in Spitsbergen was conducted under Permit 2016/00110-2 by Melanie Hopkins (American Museum of Natural History), Björn Kröger (Finnish Museum of Natural History), Seth Finnegan (University of California Berkeley), Franziska Franeck (Natural History Museum Oslo), and Håvard Kårsted (Longyearbyen), and made possible by funding from the Niarchos Foundation, the National Geographic Society, and the Societas Scientarium Fennica. This work is part of Research in Svalbard ID 10467. We thank Adam Jost and other members of the K.D.B. laboratory for substantial help with sample analysis and instrument troubleshooting. We thank the editor and two anonymous reviewers for comments on a previous version of the manuscript; their suggestions have strengthened and clarified the paper. S.L.G. was supported by a NASA Earth and Space Science Fellowship. S.F. and K.D.B. were supported by the Packard Foundation.

Downloaded at CALIFORNIA INST OF TECHNOLOGY on February 1, 2021

1. C. M. Ø. Rasmussen, B. Kröger, M. L. Nielsen, J. Colmenar, Cascading trend of Early Paleozoic marine radiations paused by Late Ordovician extinctions. *Proc. Natl. Acad. Sci. U.S.A.* **116**, 7207–7213 (2019).
2. C. R. Marshall, Explaining the Cambrian "explosion" of animals. *Annu. Rev. Earth Planet Sci.* **34**, 355–384 (2006).
3. M. R. Saltzman, C. T. Edwards, J. M. Adrain, S. R. Westrop, Persistent oceanic anoxia and elevated extinction rates separate the Cambrian and Ordovician radiations. *Geology* **43**, 807–810 (2015).
4. T. Servais, A. W. Owen, D. A. T. Harper, B. Kröger, A. Munnecke, The Great Ordovician biodiversification event (GOBE): The palaeoecological dimension. *Palaeogeogr. Palaeoclimatol. Palaeoecol.* **294**, 99–119 (2010).
5. D. M. Raup, J. J. Sepkoski, Mass extinctions in the marine fossil record. *Science* **215**, 1501–1503 (1982).
6. J. A. Trotter, I. S. Williams, C. R. Barnes, C. Lécuyer, R. S. Nicoll, Did cooling oceans trigger Ordovician biodiversification? Evidence from conodont thermometry. *Science* **321**, 550–554 (2008).
7. C. M. Ø. Rasmussen *et al.*, Onset of main Phanerozoic marine radiation sparked by emerging mid Ordovician icehouse. *Sci. Rep.* **6**, 18884 (2016).
8. S. Finnegan, *et al.*, The magnitude and duration of Late Ordovician–Early Silurian glaciation. *Science* **331**, 903–906 (2011).
9. E. U. Hammarlund *et al.*, A sulfidic driver for the end-Ordovician mass extinction. *Earth Planet Sci. Lett.* **331–332**, 128–139 (2012).
10. C. Zou *et al.*, Ocean euxinia and climate change "double whammy" drove the Late Ordovician mass extinction. *Geology* **46**, 535–538 (2018).
11. N. L. Swanson-Hysell, F. A. Macdonald, Tropical weathering of the Taconic orogeny as a driver for Ordovician cooling. *Geology* **45**, 719–722 (2017).
12. F. A. Macdonald *et al.*, Arc-continent collisions in the tropics set Earth's climate state. *Science* **364**, 181–184 (2019).
13. W. Buggisch *et al.*, Did intense volcanism trigger the first Late Ordovician icehouse?*Geology* **38**, 327–330 (2010).
14. T. M. Lenton, M. Crouch, M. Johnson, N. Pires, L. Dolan, First plants cooled the Ordovician. *Nat. Geosci.* **5**, 86–89 (2012).
15. T. W. Hearing *et al.*, An early Cambrian greenhouse climate. *Sci. Adv.* **4**, eaar5690 (2018).
16. N. R. McKenzie, N. C. Hughes, B. C. Gill, P. M. Myrow, Plate tectonic influences on Neoproterozoic-early Paleozoic climate and animal evolution. *Geology* **42**, 127–130 (2014).
17. H. C. Urey, Oxygen isotopes in nature and in the laboratory. *Science* **108**, 489–496 (1948).
18. R. Came *et al.*, Coupling of surface temperatures and atmospheric CO_2 concentrations during the Palaeozoic era. *Nature* **449**, 198–201 (2007).
19. R. C. Cummins, S. Finnegan, D. A. Fike, J. M. Eiler, W. W. Fischer, Carbonate clumped isotope constraints on Silurian ocean temperature and seawater δ18O. *Geochem. Cosmochim. Acta*, **140**, 241–258, 2014.
20. K. D. Bergmann *et al.*, A paired apatite and calcite clumped isotope thermometry approach to estimating Cambro-Ordovician seawater temperatures and isotopic composition. *Geochem. Cosmochim. Acta* **224**, 18–41 (2018).
21. G. A. Henkes *et al.*, Temperature evolution and the oxygen isotope composition of Phanerozoic oceans from carbonate clumped isotope thermometry. *Earth Planet Sci. Lett.* **490**, 40–50 (2018).
22. E. L. Grossman, M. M. Joachimski, "Oxygen isotope stratigraphy" in *Geologic Time Scale 2020*, F. M. Gradstein, J. G. Ogg, M. D. Schmitz, G. M. Ogg, Eds. (Elsevier, Amsterdam, Netherlands, 2020), pp. 279–307.
23. S. B. Pruss, S. Finnegan, W. W. Fischer, A. H. Knoll, Carbonates in skeleton-poor seas: New insights from Cambrian and Ordovician strata of Laurentia. *Palaios* **25**, 73–84 (2010).
24. J. B. D. Jaffrés, G. A. Shields, K. Wallmann, The oxygen isotope evolution of seawater: A critical review of a long-standing controversy and an improved geological water cycle model for the past 3.4 billion years. *Earth Sci. Rev.* **83**, 83–122 (2007).
25. J. Veizer *et al.*, 87Sr/86Sr, δ13C, and δ18O evolution of Phanerozoic seawater. *Chem. Geol.* **161**, 59–88 (1999).
26. J. M. Eiler, "Clumped-isotope" geochemistry—the study of naturally-occurring, multiply-substituted isotopologues. *Earth Planet Sci. Lett.* **262**, 309–327 (2007).
27. J. M. Eiler, Paleoclimate reconstruction using carbonate clumped isotope thermometry. *Quat. Sci. Rev.* **30**, 3575–3588 (2011).
28. K. D. Bergmann, S. A. K. A. L. Balushi, T. J. Mackey, J. P. Grotzinger, J. M. Eiler, A 600-million-year carbonate clumped-isotope record from the Sultanate of Oman. *J. Sediment. Res.* **88**, 960–979 (2018).
29. N. Galili *et al.*, The geologic history of seawater oxygen isotopes from marine iron oxides. *Science* **365**, 469–473 (2019).
30. F. Hodel *et al.*, Fossil black smoker yields oxygen isotopic composition of Neoproterozoic seawater. *Nat. Commun.* **9**, 1453 (2018).
31. K. Muehlenbachs, The oxygen isotopic composition of the oceans, sediments and the seafloor. *Chem. Geol.* **145**, 263–273 (1998).
32. L. E. Lisiecki, M. E. Raymo, A Pliocene-Pleistocene stack of 57 globally distributed benthic δ18O records. *Paleoceanography*, **20**, 1–17 (2005).
33. S. L. Goldberg, T. M. Present, S. Finnegan, K. D. Bergmann, Carbonate clumped-isotope analyses of early Paleozoic bulk rock and brachiopod samples from Svalbard, Newfoundland, Ohio, and Gotland. EarthChem Database. https://ecl.earthchem.org/view.php?id=1716. Deposited 13 October 2020.
34. B. H. Passey, G. A. Henkes, Carbonate clumped isotope bond reordering and geospeedometry. *Earth Planet Sci. Lett.* **351-352**, 223–236 (2012).
35. C. Lee *et al.*, Lipid biomarker and stable isotopic profiles through Early-Middle Ordovician carbonates from Spitsbergen, Norway. *Org. Geochem.* **131**, 5–18 (2019).
36. P. Brandl, "Carbon and oxygen isotopes, stratigraphy, and facies of the Oslobreen group (northeast Ny Friesland, Svalbard)," Diplom-Geologe, Friedrich-Alexander-Universität Erlangen-Nürnberg, Erlangen, Germany (2009).
37. T. J. Mackey, A. B. Jost, J. R. Creveling, K. D. Bergmann, A decrease to low carbonate clumped isotope temperatures in Cryogenian strata. *AGU Adv.* **1**, e2019AV000159 (2020).
38. S. H. Williams, E. T. Burden, P. K. Mukhopadhyay, Thermal maturity and burial history of Paleozoic rocks in western Newfoundland. *Can. J. Earth Sci.* **35**, 1307–1322 (1998).
39. G. S. Nowlan, C. R. Barnes, "*Thermal maturation of Paleozoic strata in Eastern Canada from conodont colour alteration index (CAI) data with implications for burial history, tectonic evolution, hotspot tracks and mineral and hydrocarbon exploration*" (Bulletin 367, Geological Survey of Canada, Ottawa, Canada, 1987).
40. C. E. Bennett *et al.*, Oxygen isotope analysis of the eyes of pelagic trilobites: Testing the application of sea temperature proxies for the Ordovician. *Gondwana Res.* **57**, 157–169 (2018).
41. G. L. Albanesi, C. R. Barnes, J. A. Trotter, I. S. Williams, S. M. Bergström, Comparative Lower-Middle Ordovician conodont oxygen isotope paleothermometry of the Argentine Precordillera and Laurentian margins. *Palaeogeogr. Palaeoclimatol. Palaeoecol.* **549**, 109115 (2019).
42. J. A. Trotter, I. S. Williams, C. R. Barnes, P. Männik, A. Simpson. New conodont δ18O records of Silurian climate change: Implications for environmental and biological events. *Palaeogeogr. Palaeoclimatol. Palaeoecol.* **443**, 34–48, 2016.
43. S. A. Young, M. R. Saltzman, S. M. Bergström. Upper Ordovician (Mohawkian) carbon isotope (δ13C) stratigraphy in eastern and central North America: Regional expression of a perturbation of the global carbon cycle. *Palaeogeogr. Palaeoclimatol. Palaeoecol.* **222**, 53–76, 2005.
44. A. N. Sial *et al.*, Upper Cambrian carbonate sequences of the Argentine Precordillera and the Steptoean C-Isotope positive excursion (SPICE). *Gondwana Res.* **13**, 437–452 (2008).
45. A. N. Sial *et al.*, High-resolution stable isotope stratigraphy of the upper Cambrian and Ordovician in the Argentine Precordillera: Carbon isotope excursions and correlations. *Gondwana Res.* **24**, 330–348 (2013).
46. C. K. Thompson, L. C. Kah, Sulfur isotope evidence for widespread euxinia and a fluctuating oxycline in Early to Middle Ordovician greenhouse oceans. *Palaeogeogr. Palaeoclimatol. Palaeoecol.* **313-314**, 189–214 (2012).
47. F. Gomez, N. Ogle, R. Astini, R. M. Kalin, Paleoenvironmental and carbon-oxygen isotope record of Middle Cambrian carbonates (La Laja Formation) in the Argentine Precordillera. *J. Sediment. Res.* **77**, 826–842 (2007).
48. R. Wu, M. Calner, O. Lehnert, Integrated conodont biostratigraphy and carbon isotope chemostratigraphy in the Lower-Middle Ordovician of southern Sweden reveals a complete record of the MDICE. *Geol. Mag.* **154**, 334–353 (2017).
49. A. Lindskog, M. M. Costa, C. M. Ø. Rasmussen, J. N. Connelly, M. E. Eriksson, Refined Ordovician timescale reveals no link between asteroid breakup and biodiversification. *Nat. Commun.* **8**, 14066 (2017).
50. Y. Zhang, A. Munnecke, Ordovician stable carbon isotope stratigraphy in the Tarim Basin, NW China. *Palaeogeogr. Palaeoclimatol. Palaeoecol.* **458**, 154–175 (2016).
51. M. R. Saltzman *et al.*, Calibration of a conodont apatite-based Ordovician 87Sr/86Sr curve to biostratigraphy and geochronology: Implications for stratigraphic resolution. *Geol. Soc. Am. Bull.* **126**, 1551–1568 (2014).
52. A. Prokoph, G. A. Shields, J. Veizer, Compilation and time-series analysis of a marine carbonate δ18O, δ13C,87Sr/86Sr and δ34S database through Earth history. *Earth Sci. Rev.* **87**, 113–133 (2008).
53. S. E. Peters, J. M. Husson, J. Wilcots, The rise and fall of stromatolites in shallow marine environments. *Geology* **45**, 487–490 (2017).
54. F. A. Macdonald *et al.*, Bridging the gap between the foreland and hinterland II: Geochronology and tectonic setting of Ordovician magmatism and basin formation on the Laurentian margin of New England and Newfoundland. *Am. J. Sci.* **317**, 555–596 (2017).
55. B. K. Sell, L. Ainsaar, S. A. Leslie, Precise timing of the Late Ordovician (Sandbian) super-eruptions and associated environmental, biological, and climatological events. *J. Geol. Soc.* **170**, 711–714 (2013).
56. B. K. Sell *et al.*, Stratigraphic correlations using trace elements in apatite from Late Ordovician (Sandbian-Katian) K-bentonites of eastern North America. *Geol. Soc. Am. Bull.* **127**, 1259–1274 (2015).
57. J. Zachos, M. Pagani, L. Sloan, E. Thomas, K. Billups, Trends, global rhythms, aberrations in global climate 65 Ma to present. *Science* **292**, 686–693 (2001).
58. K. G. Miller *et al.*, Cenozoic sea-level and cryospheric evolution from deep-sea geochemical and continental margin records. *Sci. Adv.* **6**, eaaz1346 (2020).
59. E. J. Judd, T. Bhattacharya, L. C. Ivany, A dynamical framework for interpreting ancient sea surface temperatures. *Geophys. Res. Lett.* **47**, 1–10 (2020).
60. A. N. LeGrande, G. A. Schmidt, Global gridded data set of the oxygen isotopic composition in seawater. *Geophys. Res. Lett.* **33**, 1–5 (2006).
61. T. Westerhold *et al.*, An astronomically dated record of Earth's climate and its predictability over the last 66 million years. *Science* **369**, 1383–1387 (2020).
62. C. T. Edwards, M. R. Saltzman, D. L. Royer, D. A. Fike, Oxygenation as a driver of the Great Ordovician biodiversification event. *Nat. Geosci.* **10**, 925–929 (2017).
63. S. Yang *et al.*, Duration, evolution, and implications of volcanic activity across the Ordovician–Silurian transition in the Lower Yangtze region, South China. *Earth Planet Sci. Lett.* **518**, 13–25 (2019).
64. D. S. Jones, A. M. Martini, D. A. Fike, K. Kaiho, A volcanic trigger for the late Ordovician mass extinction? Mercury data from south China and Laurentia. *Geology* **45**, 631–634 (2017).

Downloaded at CALIFORNIA INST OF TECHNOLOGY on February 1, 2021

65. Q. Gong, X. Wang, L. Zhao, S. E. Grasby, Z.-q. Chen, Mercury spikes suggest volcanic driver of the Ordovician-Silurian mass extinction. *Sci. Rep.* **7**, 5304 (2017).
66. D. P. G. Bond, S. E. Grasby, Late Ordovician mass extinction caused by volcanism, warming, and anoxia, not cooling and glaciation. *Geology* **48**, 777–781 (2020).
67. R. A. Fortey, L. R. M. Cocks, Late Ordovician global warming—the Boda event. *Geology* **33**, 405–408 (2005).
68. C. T. Lee, S. Dee, Does volcanism cause warming or cooling?*Geology* **47**, 687–688 (2019).
69. B. Kröger, S. Finnegan, F. Franeck, M. J. Hopkins, The Ordovician succession adjacent to Hinlopenstretet, Ny Friesland, Spitsbergen. *Am. Mus. Novit.* **3882**, 1–28 (2017).
70. R. A. Fortey, D. L. Bruton, Cambrian-Ordovician rocks adjacent to Hinlopenstretet, North Ny Friesland, Spitsbergen. *Geol. Soc. Am. Bull.* **84**, 2227–2242 (1973).
71. O. Lehnert, S. Stouge, P. Brandl, Conodont biostratigraphy in the Early to Middle Ordovician strata of the Oslobreen Group in Ny Friesland, Svalbard. *Z. Dtsch. Ges. Geowiss.* **164**, 149–172 (2013).
72. Å. Johansson, D. G. Gee, A. N. Larionov, Y. Ohta, A. M. Tebenkov, Grenvillian and Caledonian evolution of eastern Svalbard—a tale of two orogenies. *Terra. Nova* **17**, 317–325 (2005).
73. I. Knight, K. Azmy, W. D. Boyce, D. Lavoie, Tremadocian carbonate rocks of the lower St. George group, Port Au Port Peninsula, western Newfoundland: Lithostratigraphic setting of diagenetic, isotopic and geochemistry studies. *Curr. Res.*, 115–149 (2008).
74. D. Lavoie, E. T. Burden, D. Lebel, Stratigraphic framework for the Cambrian-Ordovician rift and passive margin successions from southern Quebec to western Newfoundland. *Can. J. Earth Sci.* **40**, 177–205 (2003).
75. S. R. Stenzel, I. Knight, N. P. James, Carbonate platform to foreland basin: Revised stratigraphy of the Table Head Group (Middle Ordovician), western Newfoundland. *Can. J. Earth Sci.* **27**, 14–26 (1990).
76. L. Quinn, S. H. Williams, D. A. T. Harper, E. N. K. Clarkson, Late Ordovician foreland basin fill: Long point group of onshore western Newfoundland. *Bull. Can. Petrol. Geol.* **47**, 63–80 (1999).
77. M. Cooper *et al.*, Basin evolution in western Newfoundland; new insights from hydrocarbon exploration. *AAPG Bull.* **85**, 393–418 (2001).
78. C. R. van Staal, S. M. Barr, "Lithospheric architecture and tectonic evolution of the Canadian Appalachians and associated Atlantic margin" in *Tectonic Styles in Canada: The LITHOPROBE Perspective*. J. A. Percival, F. A. Cook, R. M. Clowes, Eds. (*GAC Special Paper 49*, Geological Association of Canada, St. Johns, Canada, 2012), pp. 41–95.
79. S. M. Holland, Sequence stratigraphy of a carbonate-clastic ramp: The Cincinnatian Series (Upper Ordovician) in its type area. *Geol. Soc. Am. Bull.* **105**, 306–322 (1993).
80. M. C. Pope, J. F. Read, "High-resolution stratigraphy of the Lexington Limestone (Late Middle Ordovician), Kentucky, USA: A cool-water carbonate-clastic ramp in a tectonically active foreland basin" in *Cool-Water Carbonates*, N. P. James, J. A. D. Clarke, Eds. (Special Publications of SEPM, SEPM Society for Sedimentary Geography, Tulsa, OK, 1997), vol. 56, pp. 411–429.
81. A. Munnecke, C. Samtleben, T. Bickert, The Ireviken Event in the lower Silurian of Gotland, Sweden—relation to similar Palaeozoic and Proterozoic events. *Palaeogeogr. Palaeoclimatol. Palaeoecol.* **195**, 99–124 (2003).
82. C. Samtleben, A. Munnecke, T. Bickert, J. Pätzold, The Silurian of Gotland (Sweden): Facies interpretation based on stable isotopes in brachiopod shells. *Geol. Rundsch.* **85**, 278 (1996).
83. T. M. Present, G. Paris, A. Burke, W. W. Fischer, J. F. Adkins, Large carbonate associated sulfate isotopic variability between brachiopods, micrite, and other sedimentary components in Late Ordovician strata. *Earth Planet Sci. Lett.* **432**, 187–198 (2015).
84. C. M. John, D. Bowen, Community software for challenging isotope analysis: First applications of 'Easotope' to clumped isotopes. *Rapid Commun. Mass Spectrom.* **30**, 2285–2300 (2016).
85. S. M. Bernasconi *et al.*, Reducing uncertainties in carbonate clumped isotope analysis through consistent carbonate-based standardization. *Geochem. Geophys. Geosystems* **19**, 2895–2914 (2018).
86. S.-T. Kim, J. R. O'Neil, Equilibrium and nonequilibrium oxygen isotope effects in synthetic carbonates. *Geochem. Cosmochim. Acta* **61**, 3461–3475 (1997).
87. J. Horita, Oxygen and carbon isotope fractionation in the system dolomite-water-CO_2 to elevated temperatures. *Geochem. Cosmochim. Acta* **129**, 111–124 (2014).
88. R.-c. Wu, M. Calner, L. Oliver, O. Peterffy, M. M. Joachimski, Lower–Middle Ordovician δ13C chemostratigraphy of western Baltica (Jämtland, Sweden). *Palaeoworld* **24**, 110–122 (2015).
89. P. M. Myrow *et al.*, Ordovician–Silurian boundary strata of the Indian Himalaya: Record of the latest Ordovician Boda event. *Geol. Soc. Am. Bull.* **131**, 881–898 (2019).
90. E. Pucéat *et al.*, Revised phosphate–water fractionation equation reassessing paleotemperatures derived from biogenic apatite. *Earth Planet Sci. Lett.* **298**, 135–142 (2010).
91. K. Azmy, D. Lavoie, High-resolution isotope stratigraphy of the lower Ordovician St. George group of western Newfoundland, Canada: Implications for global correlation. *Can. J. Earth Sci.* **46**, 403–423 (2009).
92. S. Scorrer, K. Azmy, S. Stouge, Carbon-isotope stratigraphy of the Furongian Berry Head Formation (Port au Port Group) and Tremadocian Watts Bight Formation (St. George Group), western Newfoundland and the correlative significance. *Can. J. Earth Sci.* **56**, 223–234 (2019).
93. K. L. Batten Hender, "Mixed siliciclastic-carbonate ramp sediments and coral bioherms of the late Ordovician Lourdes formation, western Newfoundland: Sedimentology, stratigraphy, and tectonic significance" Ph.D. dissertation, Carleton University, Ottawa, Canada (2007).
94. A. Mauviel, A. Desrochers, A high-resolution, continuous δ13C record spanning the Ordovician–Silurian boundary on Anticosti Island, eastern Canada. *Can. J. Earth Sci.* **801** 795–801 (2016).
95. P. I. McLaughlin *et al.*, Refining 2 km of Ordovician chronostratigraphy beneath Anticosti Island utilizing integrated chemostratigraphy. *Can. J. Earth Sci.* **53**, 865–874 (2016).
96. M. R. Saltzman *et al.*, Pulse of atmospheric oxygen during the late Cambrian. *Proc. Natl. Acad. Sci. U.S.A.*, **108**, 3876–3881 (2011).
97. P. C. Quinton, A. D. Herrmann, S. A. Leslie, K. G. Macleod, Carbon cycling across the southern margin of Laurentia during the late Ordovician. *Palaeogeogr. Palaeoclimatol. Palaeoecol.* **458**, 63–76 (2016).
98. D. Kaljo, L. Hints, T. Martma, J. Nolvak, A. Oraspold, Late Ordovician carbon isotope trend in Estonia, its significance in stratigraphy and environmental analysis. *Palaeogeogr. Palaeoclimatol. Palaeoecol.* **210**, 165–185 (2004).
99. L. Ainsaar, T. Meidla, "Ordovician carbon isotopes" in *Männamaa (F-367) Drill Core, Estonian Geological Sections*, A. Põldvere, Ed. (Bulletin 9, Geological Survey of Estonia, Tallinn, Estonia, 2008), pp. 27–29.
100. S. Peng, L. E. Babcock, R. A. Cooper. "The Cambrian period" in *The Geologic Time Scale 2012*, F. M. Gradstein, J. G. Ogg, M. D. Schmitz, G. M. Ogg, Eds. (Elsevier B.V., Amsterdam, Netherlands, 2012), vol. 1–2, pp. 437–488.
101. R. A. Cooper, P. M. Sadler, "The Ordovician period" in *The Geologic Time Scale 2012*, F. M. Gradstein, J. G. Ogg, M. D. Schmitz, G. M. Ogg, Eds. (Elsevier B.V., Amsterdam, Netherlands, 2012), vol. 1–2, pp. 489–523.

Downloaded at CALIFORNIA INST OF TECHNOLOGY on February 1, 2021